Research Square

Preprints are preliminary reports that have not undergone peer review.
They should not be considered conclusive, used to inform clinical practice,
or referenced by the media as validated information.

Synthesis, Characterization, and GGA+U Electronic Structure Calculations of Hexagonal Covellite (CuS) Nanoparticles for Optoelectronic and Photothermal Applications

Hussam Musleh

hussam.musleh@univ-littoral.fr

Université du littoral côte d'opale

Samy Mansy

University College of Science and Technology - Khan Younis

Jehad Asad

Al Azhar University-Gaza

Naji AlDahoudi

Université de Picardie Jules Verne

Abdelylah Daoudi

Université du littoral côte d'opale

Abdelilah Lahmar

Université de Picardie Jules Verne

Sami Shaat

Islamic University of Gaza

Research Article

Keywords: CuS nanoparticles, Co-precipitation, DFT-GGA+U, Electronic structure, Optical properties and photothermal

Posted Date: August 25th, 2026

DOI: https://doi.org/10.21203/rs.3.rs-10474568/v1

License: This work is licensed under a Creative Commons Attribution 4.0 International License.
Read Full License

Additional Declarations: Competing interest reported. The authors would like to acknowledge the support of University Littoral Côte d'Opale (ULCO) the, University of Picardie Jules Verne (UPJV) and the

College de France through the PAUSE program, which hosted Musleh Hussam and Aldahoudi Naji.

Synthesis, Characterization, and GGA+U Electronic Structure Calculations of Hexagonal Covellite (CuS) Nanoparticles for Optoelectronic and Photothermal Applications

Hussam Musleh [1,2,*], Samy Mansy [3], Jehad Asad [2], Naji AlDahoudi [2,4],
Abdelylah Daoudi[1], Abdelilah Lahmar [4] and Sami Shaat[5]

[1] University Littoral Côte d'Opale, UR 4476, UDSMM, Unité de Dynamique et Structure des Matériaux Moléculaires, F-59140 Dunkerque, France.
[2]Al Azhar University-Gaza, Physics Department, Gaza, Palestine .
[3]University College of Science and Technology – Khan Younis, Department of Engineering Sciences and Applied Arts. Gaza, Palestine.
[4]Condensed Matter Physics Laboratory (LPMC), University of Picardie Jules Verne, 33 Rue Saint Leu, 80000 Amiens, France.
[5]Islamic University of Gaza, Physics Department, Gaza, Palestine.

[*]Corresponding Authors Musleh Hussam (hussam.musleh@univ-littoral.fr)

Abstract

Hexagonal covellite CuS nanoparticles were prepared using co-precipitation method and examined by experimental characterization together with first-principles calculations. X-RD confirmed the formation of a single CuS phase, while TEM observations showed nanoparticles with crystallite sizes mainly in the range of 13 to 15 nm. The band gap was about 2.36 eV. This value was close to the band gap predicted by PBE, GGA+U calculations, indicating that the selected Hubbard correction gives a reasonable description of characteristics of CuS. The density of states showed that the upper valence band is mainly influenced by Cu- 3d and S- 3p orbital hybridization. The calculated band structure also indicated a direct transition at the Γ point. Optical calculations showed a bulk plasma frequency near 4.8 eV and a strong energy-loss feature around 20.9 eV. The strong near-infrared absorption suggests that CuS nanoparticles may be useful for photothermal conversion and related p-type optoelectronic applications.

Keywords: CuS nanoparticles, Co-precipitation, DFT-GGA+U, Electronic structure, Optical properties and photothermal.

1. Introduction

Transition-metal chalcogenides Chalcogenides (T-M-Cs) are of great interest at the moment as their electronic structures, optical properties, plasmonic properties, and photothermal conversion capabilities can be adjusted according to need. T-M-Cs, copper sulfides show the most promise to researchers and manufacturers due to their stable stoichiometric phases and the electronic characteristics that can vary with changes in phase. Additionally, there are numerous different methods to produce CuS with different phases[1, 2]. The stoichiometric phases formula of binary coper sulfide system is ($Cu_{2-n}S$) which exhibits distinct compositional variations that significantly influence its crystal structure [3]. The main five phases extend from copper-rich chalcocite (Cu_2S, n = 0) and djurleite ($Cu_{1.95}S$, n = 0.05), through intermediate digenite ($Cu_{1.80}S$, n = 0.20) and anilite

($Cu_{1.75}S$, n = 0.25), to copper-deficient covellite (CuS, n = 1.00). CuS (covellite) is a common type of copper sulfide phases that forms a hexagonal crystal structure (space group $P6_3/mmc$). Research shows it is a p-type semiconductor with a band gap energy between 1.2 and 2.4 eV[4, 5]. The energy band gap depends on the method of preparing the CuS, as well as the crystallinity of the resulting CuS and the type and amount of doping[1, 6]. Due to the high degree of NIR-absorption and the exceptional photothermal stability covellite phase of copper sulfide has been identified as an important candidate for solar energy harvesting [6, 7]. Both of the properties noted above will enable the development of strong plasmonic and photothermal responses that are essential to the advancement of many different optoelectronic and energy transformation technologies, as well as tumour photothermal therapy and NIR optoelectronic technologies[8]. The high electrical mobility of CuS arises from the number of Cu vacancies present (V_{Cu}). CuS can be deposited by low-cost, simple wet chemical processes onto a variety of substrates, including glass, silicon, and Polycarbonate substrates. This properties enable the use of CuS materials in solar-cell components, as hole transport layers for the stable functioning of p-i-n perovskite solar cells and flexible electronic devices [9]. Otherwise, theoretical studies of the various phases of CuS have been completed using density functional theory (DFT); however, calculations completed using the generalized gradient approximation (GGA) have significantly underestimated the predicted energy band gap for CuS [10, 11]. The theoretically predicted energy band gap is significantly lower than the experimentally determined energy band gap due to the fact that GGA does not properly represent localized electrons present in Cu- 3d states [12]. The introduction of CuS through the use of the GGA+U method incorporates on-site Coulomb interactions, thereby improving the correlation of d electrons and increasing the reliability of the predicted electronic and optical properties of CuS. Recent first-principles studies with accurate Hubbard corrections have reproduced key optical and electronic properties of Cu -based chalcogenides [13]. Despite these advances, systematic studies correlating experimentally synthesized CuS nanoparticles with calibrated GGA+U calculations remain scarce. Previous works mainly treated either electronic band structure [10, 11], or optical and plasmonic response in CuS nano-structures [14, 15], whereas a fully integrated experimental-theoretical framework remains limited. Direct correlation between hexagonal covellite CuS nanoparticles and calibrated PBE-GGA+U calculations, including band structure, orbital-resolved density of states, dielectric response, reflectivity, refractive index, and energy-loss function over a broad photon-energy range needs further investigation. The novelty of this work is to establish a coherent experimental-computational approach connecting the structural, electronic, and optical properties of hexagonal CuS nanoparticles and clarifying their plasmonic photothermal response [8, 13]. Such a framework is essential for evaluating their NIR-driven photothermal and optoelectronic potential [16, 17]. In this work, covellite-phase CuS nanoparticles were synthesized in powder form by a chemical precipitation route. Their structural and optical properties were experimentally investigated and complemented by first-principles calculations within the PBE-GGA+U framework to capture Cu-3d correlation effects accurately. The experimental results were compared with those obtained from PBE-GGA+U computational approach.

2. Synthesis of copper sulphide (CuS) nanoparticles in covellite phase

The synthesis of copper sulphide (CuS) nanoparticles in covellite phase was carried out via a chemical precipitation route using Copper(II) acetate anhydrous, ($Cu(CH_3COO)_2$, 99.9%) and Thiourea (NH_2CSNH_2, 99.9%).

In a typical procedure, a 100 mM aqueous solution of Copper(II) acetate anhydrous, serving as the copper source ($3d^{10}$,$4s^1$, provides Cu^{2+} ions). Subsequently, a 600 mM aqueous solution of sodium thiosulfate was added dropwise to the copper acetate aqueous solution. Where, sodium thiosulfate serving as the sulfur source ($3s^2$, $3p^4$, provides S^{2-} ions). As the Cu^{2+} ions are liberated, they immediately seek out the S^{2-} ions in the solution to form the precipitate as illustrated in eqn.1. The resulting mixture was subjected to continuous magnetic stirring at a constant temperature of about 85-90 °C for a duration of 6 hours[1].

$$S^{2-}(aq.) + Cu^{2+}(aq.) \rightarrow CuS\,(aq.) \qquad (1)$$

During this process, the colour of the mixture changed to dark blue indicating the formation of CuS precipitates. After the reaction was complete, the precipitates was collected and purified through five washing cycles using centrifugation; about 4300 rpm, to remove any unreacted precursors. Finally, the obtained material was dried to yield the final CuS powder, which was then used for further characterizations. The synthesis procedure was illustrated in Fig.1.

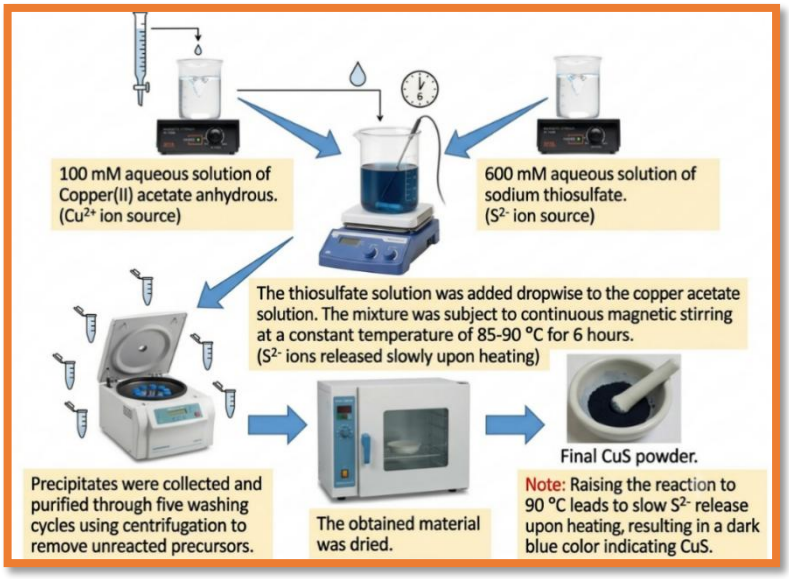


Fig.1. : The steps involved in synthesizing CuS NPs.

3. Characterization

The crystal structure of the as- prepared samples was investigated over the range of wide Bragg's angle (2θ = 10 – 80 degrees) using a Bruker D8 Discover instrument with a Cu Ka beam at 40 kV

and 15 mA with λ=1.5406 Å radiation. The morphological characteristics of the nanoparticles have been studied using JOEL-JEM-2100 transmission electron microscope (TEM), 200 kV, which combines with an PC system. TEM specimens were prepared by dissolving and subsequent drying of some drops of very diluted ethanolic colloidal solution on a copper grid (3 mm in diameter). The optical properties of the as-prepared CuS nanoparticles were deduced from absorbance spectra were measured using a JASCO, V-670 UV–Visible spectrophotometer in the range 200–1500 nm. The Photoluminescence (PL) emission spectra were registered using SPF-200 spectrofluorometer (Biotech Engineering Management Co., UK). PL measurements were measured at room temperature using 150 W Xenon Lamp with a high sensitivity photomultiplier tube, as a detector in the range from 400 nm to 600 nm. Raman spectra were recorded using Raman spectrophotometer (Reni sha, in Via Qontor Raman Microscope) in the range 100–1200 cm^{-1}.

4. Computational approach

In this study, hexagonal CuS was investigated using first-principles calculations based on density functional theory (DFT). The electronic and optical properties were calculated using the CASTEP code implemented in Materials Studio 7.0, employing a plane-wave ultrasoft pseudopotential approach. The exchange–correlation interactions were described within the generalized gradient approximation (GGA) using the PBE functional. To properly account for the localized Cu-3d electrons, the on-site Coulomb interaction was included through the GGA+U formalism, with a Hubbard parameter U = 6.5 eV. The unit cell of CuS was fully optimized before to property calculations. The convergence criteria for geometry optimization were set to 0.01 eV/Å for the maximum force and 5.0×10^{-4} Å for the maximum atomic displacement. A plane-wave cutoff energy of 700 eV was employed, and Brillouin zone integrations were performed using a Monkhorst–Pack k-point mesh of 12 × 12 × 3. All calculations were carried out using ultra-fine quality settings to ensure numerical accuracy.

5. Results and discussion

5.1 Structural Properties

The crystal structure of the covellite, hexagonal CuS structure is shown in Fig.2. In this crystal structure, the six brown-colored atoms represent copper, while the remaining twenty-two golden-colored atoms indicate sulfur. CuS crystallizes in a hexagonal system with space group $P6_3/mmc$ (No. 194).

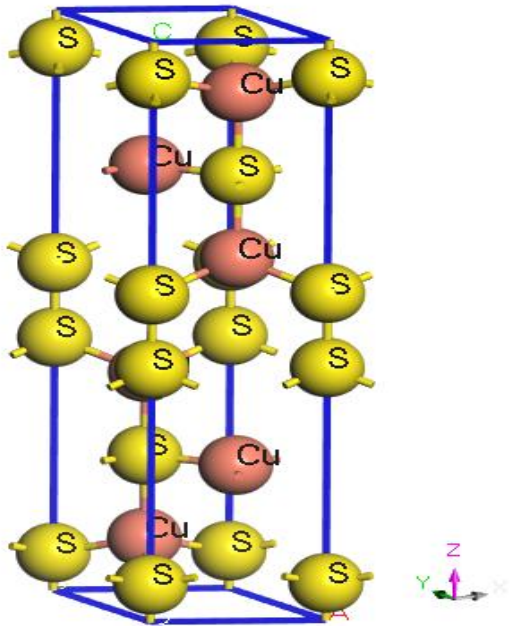


Fig. 2. : Crystal structure of a- CuS of Covellite, hexagonal

5.1.1 Identification of synthesized material

Fig. 3 shows the experimental XRD pattern of the as-synthesized CuS nanoparticles together with the simulated pattern obtained using the PBE–GGA+U functional. The pattern confirms the formation of single-phase hexagonal covellite CuS (space group $P6_3/mmc$, No. 194), consistent with references [3, 18] and the standard JCPDS card No. 78-0876 (or 06-0464). No impurity or extra peaks were detected. The main diffraction peaks at 27.164°, 27.819°, 29.446°, 31.919°, 32.039°, 48.177°, 52.86°, 58.852°, and ~59.55° correspond to the (100), (101), (102), (103), (006), (105), (110), (108), and overlapping (116)/(203) planes, respectively [5, 19]. The peaks associated with the (102), (103), and (110) planes exhibit the highest intensities, suggesting a preferred crystallographic orientation along these directions a feature frequently reported for nanostructured CuS prepared by wet-chemical methods. The noticeable peak broadening is primarily attributed to the small nanoscale crystallite size of the particles. The simulated pattern exhibits excellent agreement with the experimental peak positions, reinforcing the reliability of the GGA+U structural optimization. The obtained lattice parameters are listed in Table 1.

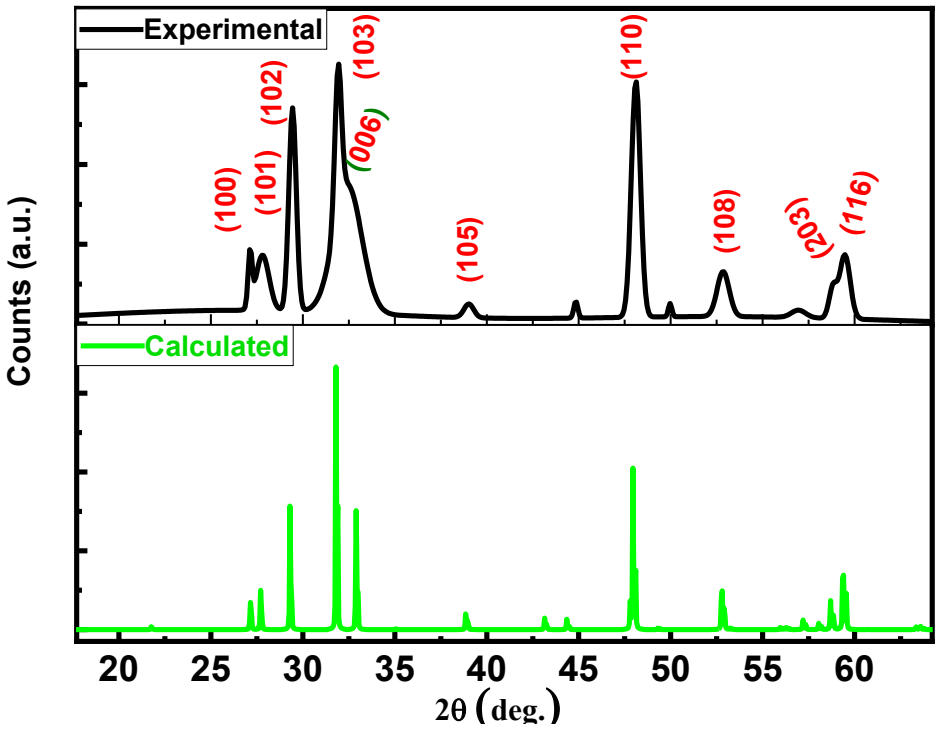


Fig. 3. : XRD patterns of covellite hexagonal CuS-NPs.: (a) experimental and (b) calculated (GGA+U).

5.1.2 Crystallite size and geometrical parameters estimation

The Debye–Scherrer method is a well-established approach for estimating the average crystallite size ($D_{AVG.}$) from the broadening of XRD diffraction peaks without taking into account the effect of microstrain. The crystallite size can be determined using the formula given in eqn.(2) [20].

$$D_{AVG.} = k\lambda/(\beta_{hkl}\, Cos\phi) \qquad (2)$$

where $D_{AVG.}$ is the average crystallite size (nm), k is the shape factor (≈0.9 for nearly spherical crystallites), λ is the X-ray wavelength of Cu Kα radiation (1.5406 Å = 0.15406 nm), β_{hkl} is the full width at half maximum (FWHM) of the selected diffraction peak (in radians), and ϕ is the Bragg angle. The Debye–Scherrer analysis is presented in Fig. 4, and the average crystallite size obtained for CuS was approximately 13.9 nm. It should be noted that the Debye–Scherrer method does not explicitly account for additional peak broadening arising from lattice microstrain and crystal imperfections. Therefore, the Williamson–Hall method (WHM) under the uniform deformation model (UDM) was also applied, assuming that the total peak broadening is the sum of the size and strain contributions and that both contributions are independent [7]. The UDM is given by eqn.(3) [21]

$$\beta_{hkl} Cos(\phi) = \left(K\lambda/D_{AVG.}\right) + 4\Xi\, Sin(\phi) \qquad (3)$$

The crystallite size $D_{AVG.}$ is obtained from the y-intercept ($k\lambda/ D_{AVG.}$), whereas the micro-strain Ξ is extracted from the slope. The extracted values for CuS where $D_{AVG.} \approx 15.4$ nm and $\Xi \approx 4.6 \times 10^{-3}$. Fig. 5. show the Williamson–Hall (UDM) plot.

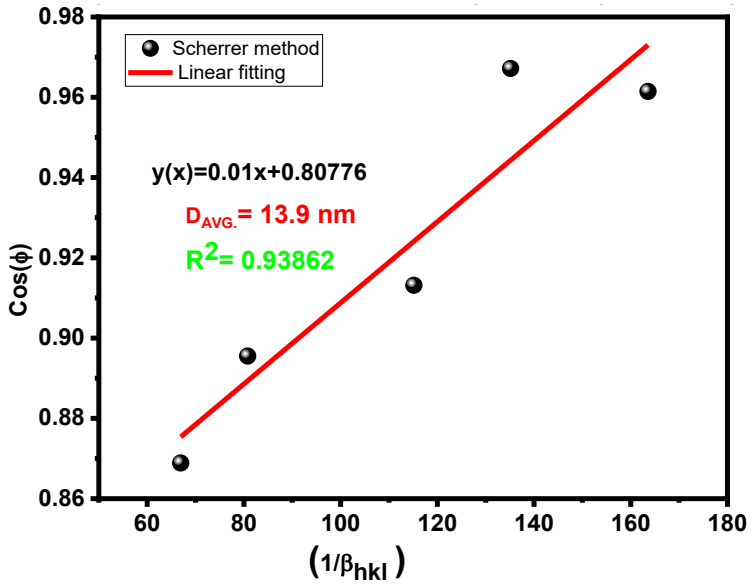


Fig. 4. : Debye Scherrer method for covellite hexagonal CuS-NPs

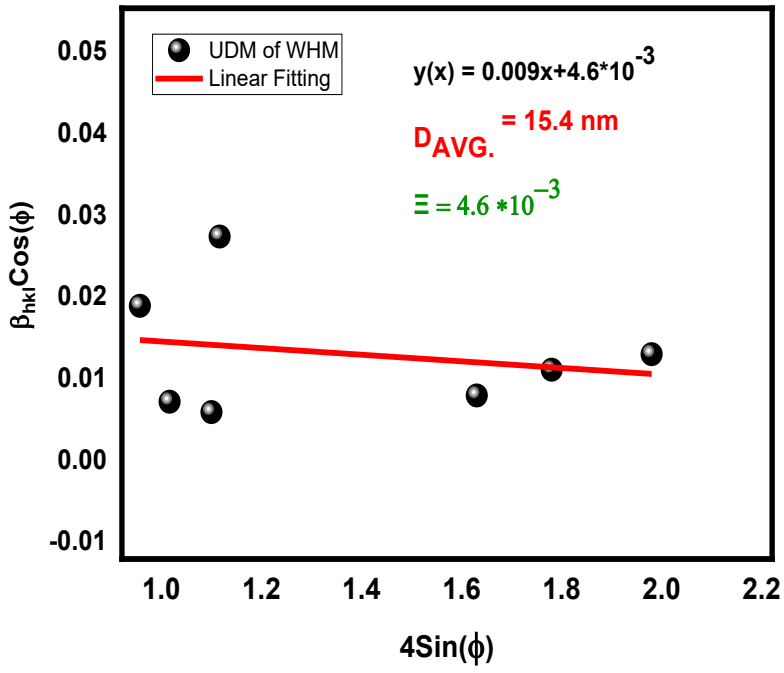


Fig. 5. : UDM analysis of WHM methods for covellite hexagonal CuS-NPs

Table 1. Summary of cohesive structural and geometric parameters for covellite hexagonal CuS-NPs

Geometric Parameters of Pure CuS NPs							Scherrer method	UDM analysis of WHM method	
#	(hkl)	(2θ)	d_{hkl} (nm)	a (Å)	c (Å)	V $(Å)^3$	$D_{AVG.}$ (nm)	$D_{AVG.}$ (nm)	Ξ $*10^{-3}$
	1 0 0	27.138	0.328						
	1 0 2	29.296	0.305						
	1 0 3	31.806	0.281						
Pure CuS	0 0 6	32.894	0.272	3.791	16.324	203.170	13.9	15.4	4.6
	1 1 0	47.953	0.190						
	1 0 8	52.777	0.173						
	1 1 6	59.374	0.156						
Reference [5]				3.790	16.340	203.260			
JCPDS card (No.78-0876)				3.791	16.324	203.724			

5.2 HRTEM analysis of CuS NPs.

The morphology, particle size distribution, and crystalline nature of the CuS NPs were investigated using high resolution transmission electron microscopy (HR-TEM). Fig. 6 shows the micrograph of the synthesized CuS NPs. As shown in Fig. 6(a), the micrograph exhibit a nearly spherical morphology of the nanoparticle with relatively uniform distribution and limited agglomeration. The particle size distribution was evaluated from the HR-TEM micrographs using a histogram, as presented in Fig. 6(b). The average particle size was estimated to be 11.12 ± 1.8 nm, which is in good agreement with the crystallite size obtained from the XRD analysis. The small particle size and non-agglomeration revealed by the the micrograph demonstrate the unique properties of the synthesized material. Specifically, its high solubility in liquids yields stable suspensions that resist sedimentation, thereby opening new avenues for various medical and industrial applications. Furthermore, the selected area electron diffraction (SAED) pattern shown in Fig. 6(c) displays well-defined diffraction rings, confirming the polycrystalline nature of the synthesized CuS NPs.

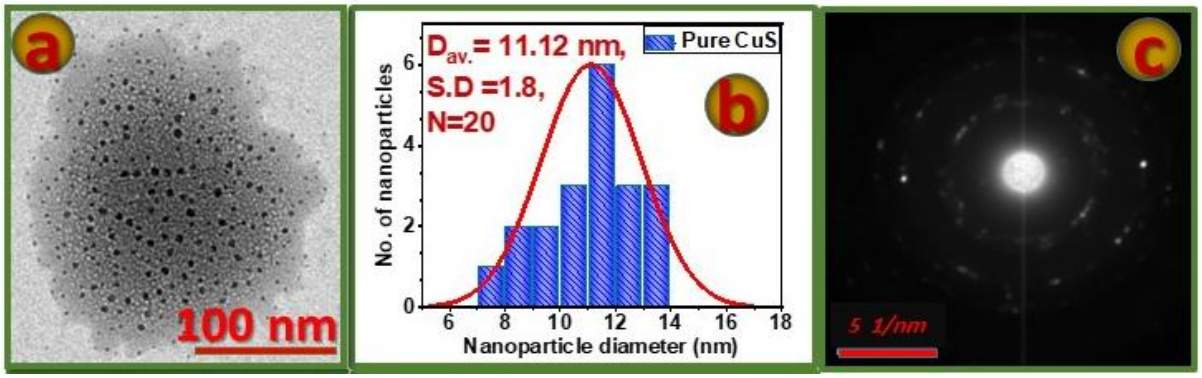


Fig. 6. : (a) micrograph image of covellite hexagonal CuS-NPs (b) histogram with a solid (line) line represents the size distribution fit to a normal function, (c) Selected area diffraction (r = 5(1/nm))

5.3 Optical properties

5.3.1 Optical energy gap

UV-Vis-NIR spectroscopy was performed to evaluate the optical response of the CuS nanoparticles synthesized from 300–1500 nm. In Figure 7(a), the experimental absorbance spectrum shows strong absorption well into the NIR region, which is a characteristic attribute of covellite CuS. The calculated spectrum is presented in Figure 7(b) shows similar trends, demonstrating good qualitative agreement with the experimental data, demonstrating the validity of the computational approach used. The strong near-infrared (NIR) absorption observed in CuS nanoparticles is consistent with recent reports on plasmon-enhanced photothermal effects in copper sulfide systems [8]. Such plasmonic behavior in semiconducting sulfides has been attributed to collective electronic oscillations arising from p–d hybridization, which is a key factor for efficient light-to-heat conversion [22]. It is clear that from Fig. 7, the intensity of the absorption of CuS nanoparticles in the NIR region is very high. This result explains the higher suitability of this material in the NIR region. This implies that the material is capable of absorbing high wavelengths coming of the solar spectrum and converting them into heat sufficient for water heating. Additionally, this material possesses the ability to absorb laser radiation at appropriate wavelengths and convert it into heat. This technique that has become widely utilized in cancer treatment.

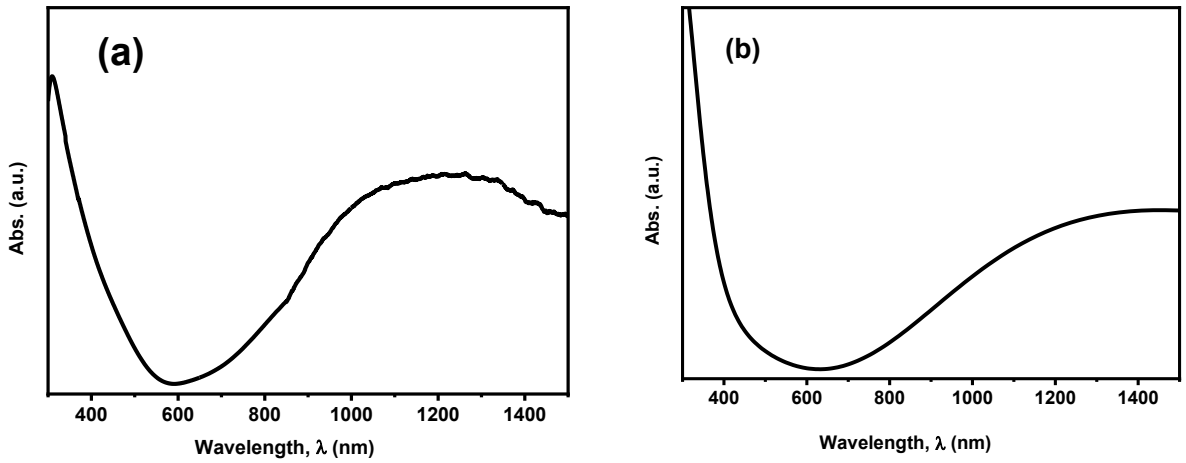


Fig. 7. : Absorption of (a), experimental and, (b) computational for covellite hexagonal CuS-NPs

Additionally, by using Tauc-Davis and Mott equation, optical energy gap (E_G) can be extracted easily using absorption spectrum [23, 24].

$$\beta hf = Æ(hf - E_G)^{\mu} \qquad (4)$$

Where, β is the absorption constant , h is the Plank's constant, f is the frequency of photon, and E_G is the optical energy gap. In our case, electronic transitions is direct allowed electronic transitions so, μ = 0.5 [25, 26]. The E_G can be determined easily by plotting $(\beta hf)^2$ versus photon energy (h*f*) and extrapolation of the linear portion of the curve to $(\beta hf)^2 = \text{zero}$. Fig. 8 shows that the determined E_G was around 2.36 ± 0.21 (eV). These findings are consistent with our computational study and the values in which urea was utilized as a fuel in the combustion technique [26]. Fig.8 displays good agreement between experimental and computational values. The strong correlation between these results reflect the effectiveness of the employed approximation and the accurize of the derived values.

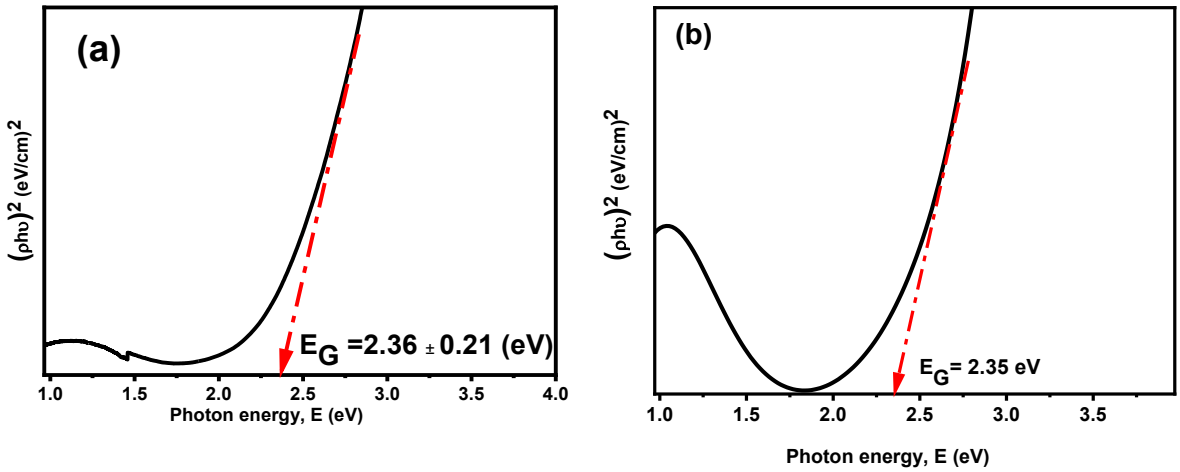


Fig. 8. : Plot of, (a) experimental and, (b) computational $(\rho h\upsilon)^2$ Vs photon energy ($h\upsilon$) for covellite hexagonal CuS-NPs

5.3.2 Raman Spectroscopy

Raman spectroscopy was employed to further confirm the phase formation and bonding characteristics of the synthesized CuS. As shown in Fig. 9, the raman spectrum exhibits a dominant and sharp band centered at ~469.7 cm^{-1}, which is characteristic of covellite CuS and is commonly attributed to vibrational modes involving the covalent S–S bonding within the crystalline lattice. In addition, a weak but distinguishable feature is observed at ~266.4 cm^{-1}, which can be associated with lattice-related vibrations (Cu–S framework modes) of the hexagonal CuS structure. The appearance of these two bands, together with the absence of extra Raman-active peaks in the measured range, is in good agreement with previously reported Raman signatures of covellite CuS, indicating successful formation of the targeted phase with good crystallinity [27, 28].

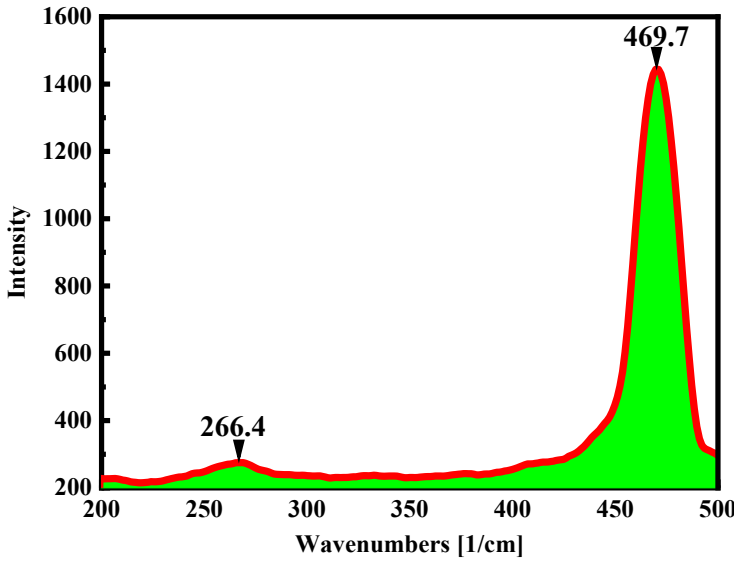


Fig. 9. : The Raman spectra of covellite hexagonal CuS-NPs

5.3.3 The photoluminescence (PL) emission

PL spectra obtained for the prepared sample are shown in Fig. 10. The sample was excited using wavelength of 320 nm. The results revealed the appearance of two peaks. The major peak is found in the range of 320-440 nm, while the second broad feature occurs between 460-500 nm. These emission features are similar to those reported in previous studies for the CuS [29], which may be derived from the recombination of electrons and holes in the surface states. PL spectrum was deconvoluted using a Gaussian function, resolving into four distinct emission peaks positioned at 344 nm (3.605 eV), 362 nm (3.427 eV), 395 nm (3.137 eV), and 475 nm (2.612 eV). The high-energy emission peaks situated in the ultraviolet (UV) region at 3.605 eV and 3.427 eV are mostly attributed to the Near Band-Edge (NBE) emission. The higher intense deconvoluted two peaks in UV region seen result from excitons (particles made up of a negatively charged electron and a positively charged hole) recombining through direct radiative processes. The significant blue shift that occurs in these band-edge emissions compared to bulk CuS would indicate that quantum confinement effects are operating on the ultra-small or thin crystalline domains found in the hexagonal covellite phase [30, 31]. The 3.137 eV peak can usually be classified as relating to shallow traps, which are only slightly below the conduction band and can be classified as deep-level emissions (DLE) or defects; therefore, generating a pathway for radiative recombination. The other significant visible green to blue (2.612eV) emission peak is generally attributed to existing lattice defects found within the covellite structure. These include the presence of copper vacancies (V_{Cu}) or sulfur interstitials (I_S), giving rise to the possibility for radiative recombination paths via deep defect trap levels in the forbidden bandgap [32]. Therefore, defect profile characteristics have a very important role to play in practical applications such as photocatalysis[30, 31].

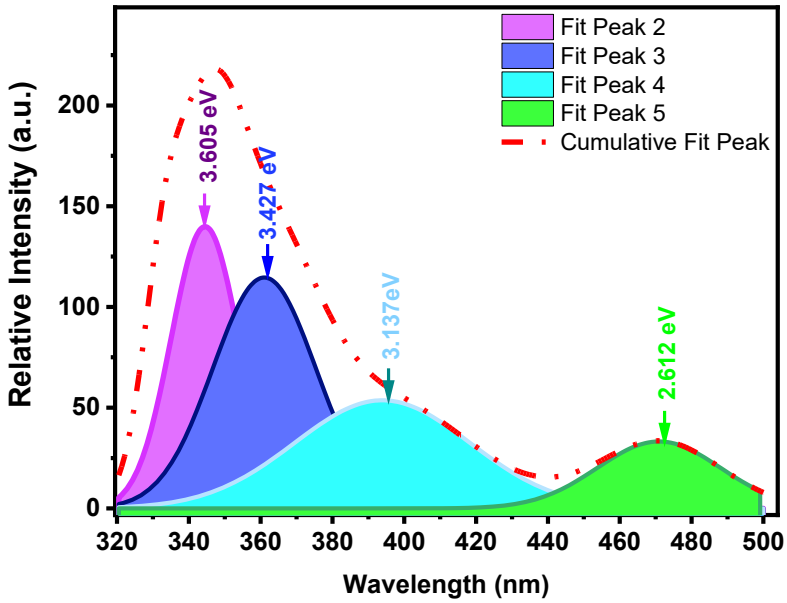


Fig. 10. : The deconvoluted photoluminescence (PL) emission of covellite hexagonal Covellite CuS-NPs at room temperature.

5.4 Density of states and energy band structure

To clarify the electronic properties of hexagonal CuS, first-principles DFT calculations (with PBE-GGA) was used to obtain the total density of states (ΓDOS), partial density of states (ΎPDOS), electronic band structure that identifies the predominant orbitals, and helps to identify the type of band gap [33]. Examination of the (ΎPDOS) profile (Figure 11) indicates that the deep valence band region (-13 eV) is primarily due to localized S-3s states which have little participation in the electronic conduction process [11]. On the other hand, the upper valence band nearest to the fermi level is principally the product of strong hybridization of Cu-3d and S-3p orbitals, suggesting the significance of p-d orbital interactions in forming the valence electronic structure, and confirming the covalent character (Cu-S bonding) in covellite CuS [34]. The result of the calculated ΓDOS can be seen in Figure 12 and further confirms the semiconductor properties of hexagonal CuS. The presence of an electronic state density at the Fermi level is indicative of a lack of metallic conduction under equilibrium conditions. The calculated band gap also closely matches the experimental optical band gap, with values of 2.36 eV for each. This indicates the accuracy of the GGA+U method in describing the localized Cu-3d states, as well as improving the electronic structure of CuS compared to results obtained using conventional GGA calculations. Contributions to the electron transitions in the conduction band region will largely come from Cu-derived states, particularly the 3p and portions of the 3d orbital from copper; while S-p states will have some role as well. The electronic band structure, shown in Figure 13, supports the DOS analysis and shows both the VBM and CBM at the Γ point, thereby providing evidence of a direct transition (Γ-Γ) with a band gap of 2.36 eV [35]. The direct band-gap nature is advantageous for optoelectronic

applications because it facilitates optical absorption and electron-hole transition processes. Overall, the combined (ΓDOS), (PDOS), and band-structure results demonstrate that hexagonal covellite CuS behaves as a direct band-gap semiconductor, with its electronic properties mainly controlled by strong Cu-3d and S-3p hybridization[36].

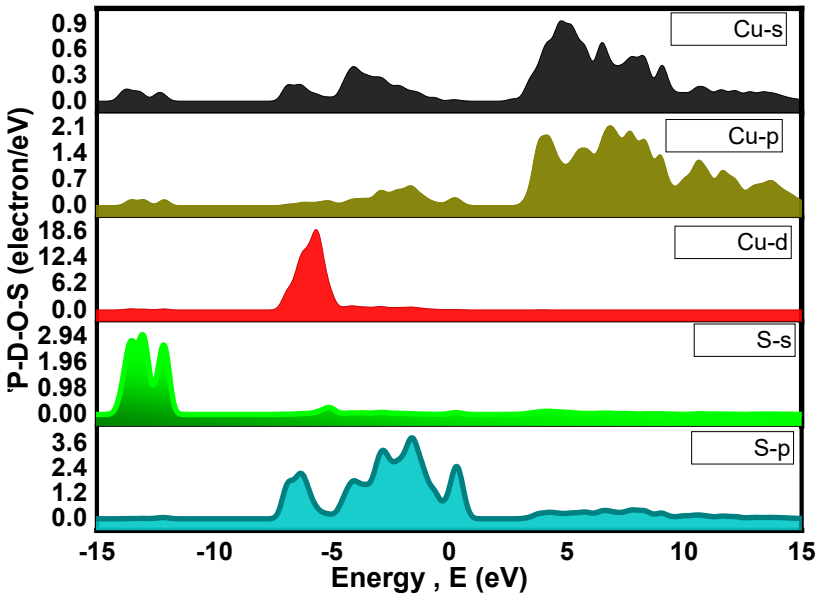


Fig. 11. : Calculated partial density of states (ΓPDOS) for covellite hexagonal CuS-NPs using the PBE-GGA functional.

.

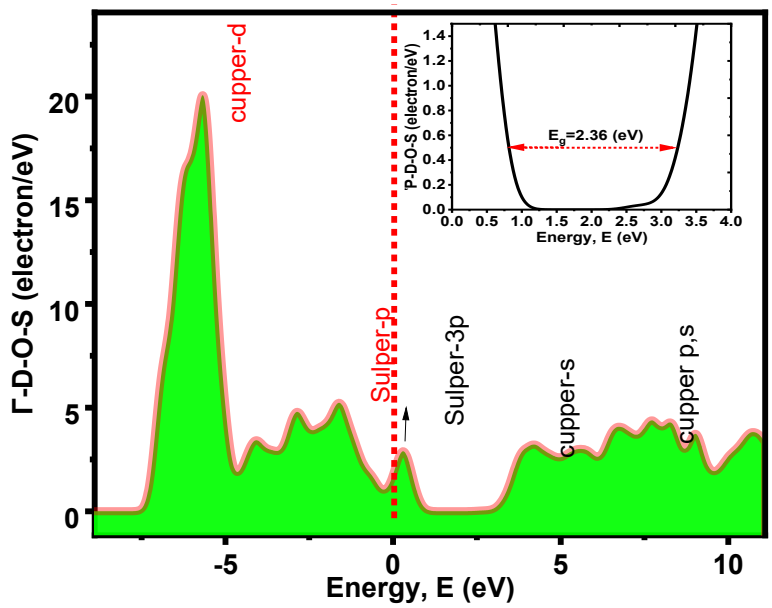


Fig. 12. : Calculated total density of states (ΓDOS) for covellite, hexagonal CuS structure.

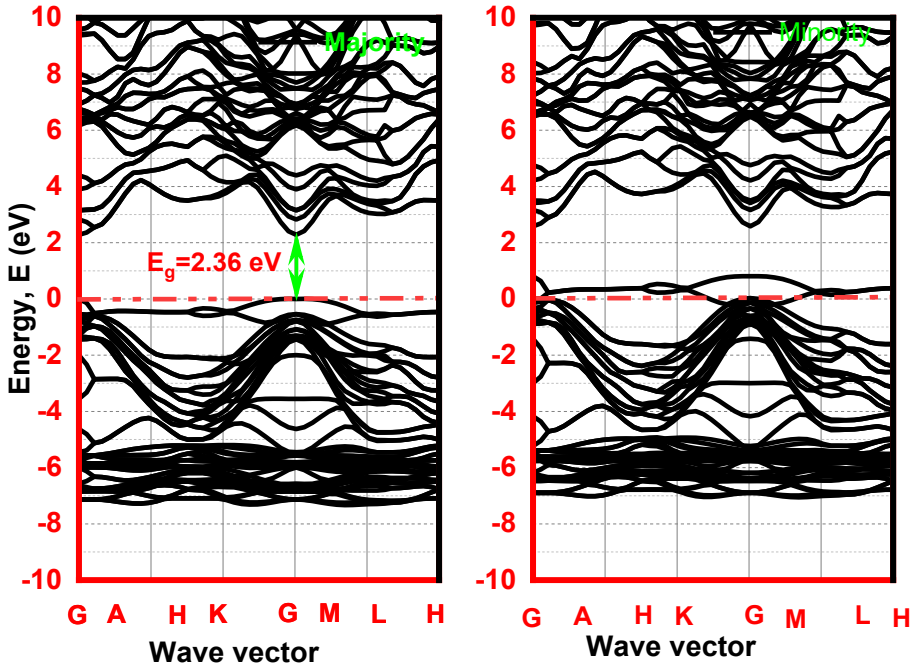


Fig. 13. : Calculated electronic band structure for the (a) majority and (b) minority electrons of covellite, hexagonal CuS structure.

5.5 The optical dielectric functions

The optical dielectric function $\varepsilon(\omega)$, is a complex quantity that describes the behavior of semiconductor materials respond to external electromagnetic waves, primarily light. Significantly, it acts as a bridge connecting macroscopic optical properties to the material's microscopic electronic structure [7]. The optical response of hexagonal CuS is governed by its complex dielectric function[37]:

$$\varepsilon(\omega) = \varepsilon_1(\omega) + I\varepsilon_2(\omega) \qquad (5)$$

As illustrated in Fig. 14, the real part $\varepsilon_1(\omega)$ is positive in the low-energy region, which is characteristic of semiconducting behavior. At zero energy (DC limit) the static permittivity ε(ω=0) about 5.63. At this point, the polarization is large, causing the material to store the maximum possible amount of electrical energy [38]. The higher peak located around 4.89 eV, $\varepsilon_1(\omega)$ illustrated the major peak about 4.89 eV, indicating higher polarization and strong redistribution of charges. From (7.83 – less than 19.19 eV), the material is unable to allow the electric field to penetrate the material easily. This results in a strong reflection of the electromagnetic waves incident upon it behaving similarly to a mirror for light, the material behaves in this region like Left- Handed Materials [39]. The imaginary part ε₂(ω) remains negligible below the band gap (~2.35 eV), consistent with the absence of optical absorption in this region. Above the band edge, ε₂(ω) increases sharply due to allowed inter-band transitions between the valence and conduction bands, which are dominated by Cu–d and s–p hybridized orbitals. This dielectric behavior aligns well with previous optical studies on copper sulfides[14, 40] .

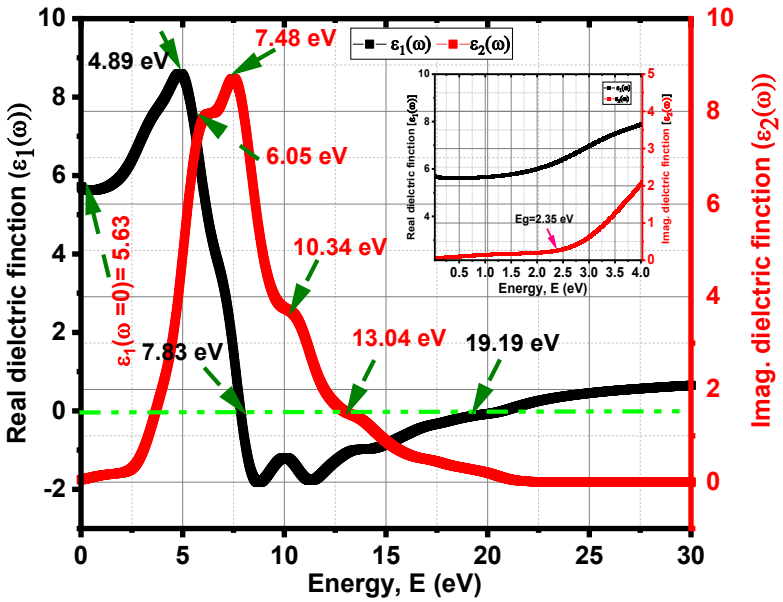


Fig. 14. : Calculated real and complex part for dielectric functions (ε(ω)) for covellite, hexagonal CuS structure.

5.6 Reflectivity

The reflectivity spectrum of CuS (Fig.15) is directly linked to its dielectric response via the Fresnel formalism and thus mirrors the material's intrinsic electronic structure[41]. The normal-incidence reflectivity is given by Fresnel's formula[7]:

$$R(\omega) = \left| \frac{\sqrt{(\varepsilon(\omega))} - 1}{\sqrt{(\varepsilon(\omega))} + 1} \right|^2 \quad (6)$$

The R(0) measured at zero reflectivity of 0.17 implies very little reflection is occurring at low photon energies. This illustrated behavior is typical for semiconductor materials but not metals. The most significant maximum in the R(ω) curve occurs at a photon energy of approximately 15.57 eV and is immediately followed by a prominent decrease in reflectivity near 20.7 eV. The energy at which the sharp drop occurs corresponds precisely with the location of the main peak in the energy-loss function shown in Section 5.8. This indicates very efficient plasmon excitation at that energy. Plasmonic conduction will entirely suppress the ability of the material to reflect light beyond the plasma frequency because plasmonic excitation creates effective dissipation of energy from collective electron oscillations (or plasmons). Thus, while the reflectivity spectrum is not an independent property, it is a reflection of the dielectric constant's zero-crossing condition at $\varepsilon_1(\omega) = 0$ and the associated plasmon resonance found in the energy-loss function[42].

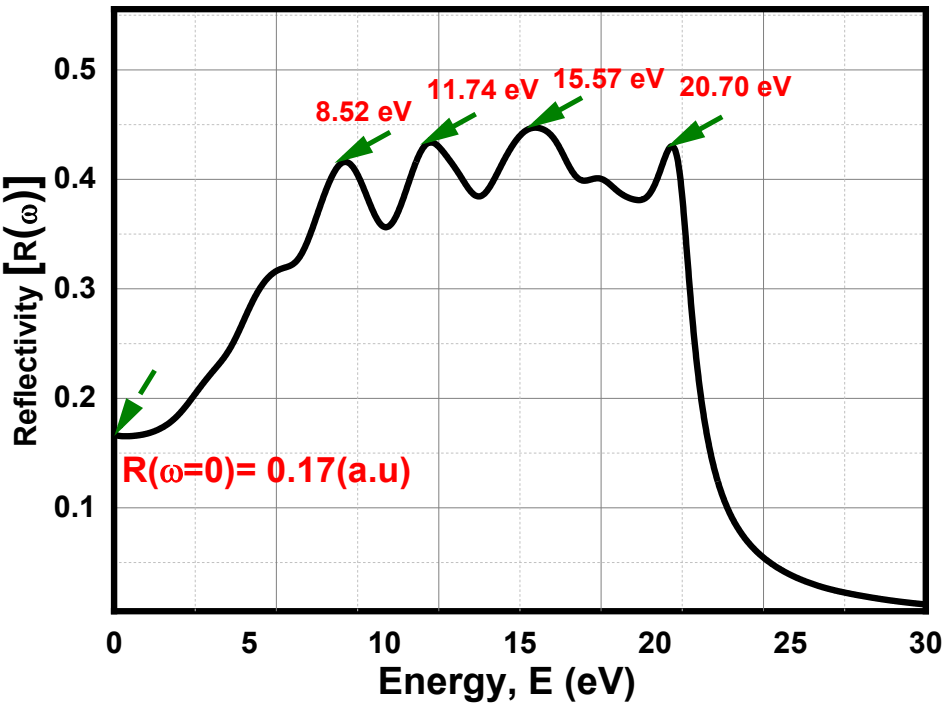


Fig. 15. : Calculated the reflectivity for covellite hexagonal CuS-NPs.

5.7 The refractive index n(ω)

The complex refractive index n(ω) provides complementary information about light propagation and absorption mechanisms [43]. The optical response of hexagonal CuS is governed by, the real $\Lambda(\omega)$, complex $\Lambda(\omega)$ and total refractive index $\mathrm{n}(\omega)$ is utilized by the Eqs. (7), (8), and (9) [44]:

$$\mathrm{n}(\omega) = \Lambda(\omega) + \mathrm{I}\,\check{\mathrm{k}}(\omega) \qquad (7)$$

$$\Lambda(\omega) = (2)^{-0.5}\left\{\left(\varepsilon_1^2(\omega) + \varepsilon_2^2(\omega)\right)^{0.5} + \varepsilon_1(\omega)\right\}^{0.5} \qquad (8)$$

$$\check{\mathrm{k}}(\omega) = (2)^{-0.5}\left\{\left(\varepsilon_1^2(\omega) - \varepsilon_2^2(\omega)\right)^{0.5}\varepsilon_1(\omega)\right\}^{0.5} \qquad (9)$$

The Plots of calculated data refractive index($\Lambda(\omega)$ and extinction coefficient $\check{k}(\omega)$, for covellite hexagonal CuS-NPs is illustrated in Fig. 16. The real part exhibits moderate dispersion in the low-energy region, reflecting normal dielectric polarization in a semiconducting medium. Static refractive index $\Lambda(\omega = 0) = 2.38$. The refractive index ($\Lambda(\omega)$ black curve) shows dispersion behavior, peaking around 6 eV before dropping sharply as it enters the inter-band absorption region. The extinction coefficient $\check{k}(\omega)$ remains nearly zero below the fundamental band gap (~2.35 eV), further confirming the absence of electronic transitions in this region. Above this threshold, $\check{k}(\omega)$increases sharply due to inter-band optical transitions, consistent with the rapid growth of $\check{k}(\omega)$. The observed absorption peaks at higher energies correspond to transitions involving Cu–d and s–p derived states, in agreement with the Γ-D-O-S analysis presented earlier. Thus, the refractive index behavior strongly reinforces the semiconducting nature of CuS while reflecting the influence of plasmonic excitations at higher photon energies.

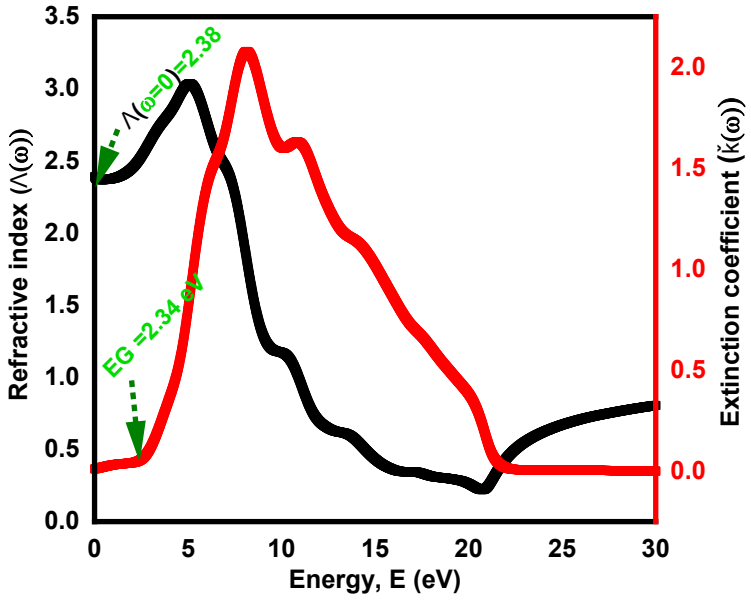


Fig. 16. : Plots of calculated data refractive index and extinction coefficient, for covellite hexagonal CuS-NPs.

5.8 Loss function

The energy-loss function (L) describes the energy dissipated by fast electrons traversing the material and is particularly sensitive to plasmon excitations [23, 33]. It is formally defined as:

$$L(\omega) = IM[-\{\varepsilon(\omega)\}^{-1}] = IM[-\{\varepsilon_1(\omega) + I\,\varepsilon_2(\omega)\}^{-1}] \qquad (8)$$

Fig. 17. Illustrates a very strong, narrow peak (around 20.9 eV) in the spectrum of hexagonal CuS is due to the bulk plasmon resonance of CuS. This energy corresponds to where the permittivity becomes equal to zero, which is also where the reflectance has a sudden drop-off in value, indicating that this excitation occurs collectively. The very strong loss peak suggests a highly efficient collective oscillation of the valence electrons, which are largely due to the Cu-derived states. There is no contradiction with this finding and with the conclusions made by the theoretical electronic band structure calculation that hexagonal CuS is in a semiconducting ground state, as this excitation occurs at a much higher energy than the band gap. Therefore, since all of these properties (absolute dielectric zero crossing, reflectivity suppression and very large loss peak) correspond to the conclusion that hexagonal CuS has semiconducting character and displays a high-energy plasmonic potential, rather than exhibiting metallic conduction.

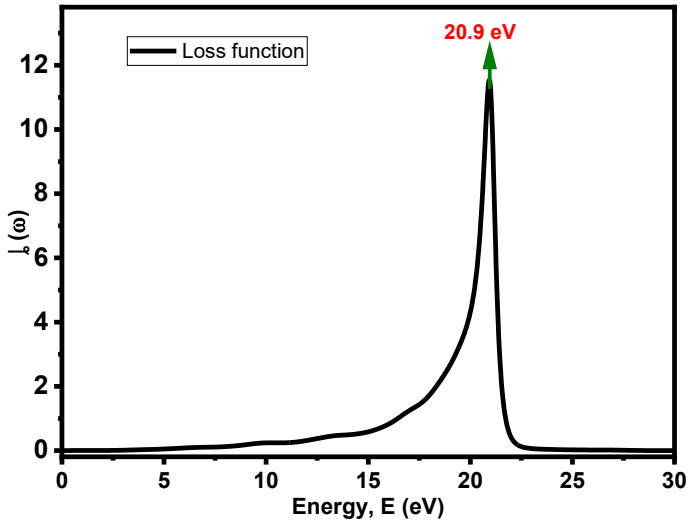


Fig. 17. : Calculated the loss function for covellite hexagonal CuS-NPs

6. Conclusion

Hexagonal covellite (CuS) nanoparticles were successfully synthesized through a controlled co-precipitation method and their properties were examined using some of experimental techniques & PBE-GGA+U first-principles approach. Calculations using both Debye-Scherrer and Williamson-Hall indicate that the crystallite size consistently falls within the 13.9 –15.4 nm. While the internal stress (microstrain) value is approximately $4.6X10^{-3}$. These convergent results validate the accuracy of the estimated parameters. TEM observations further revealed nearly spherical nanoparticles with limited agglomeration, while the SAED pattern confirmed the polycrystalline nature of the synthesized CuS nanoparticles. Raman spectroscopy, with characteristic bands near 266.4 and 469.7 cm^{-1}, supported the formation of covellite CuS and

confirmed the Cu–S/S–S bonding features, whereas PL emission bands in the 320–400 and 460–500 nm regions were attributed to electron–hole recombination involving surface-related states. The results of the UV–Vis–NIR study indicated that there is a high degree of absorption going beyond 700 nm into the near-infrared region and demonstrated a direct optical band gap of 2.36 ± 0.21 eV (close to the calculated PBE–GGA+U estimate of ~2.35 to 2.36 eV). The electronic band structure indicated a direct transition between the Gamma points (Γ–Γ transition) due to the presence of a high degree of Cu-3d/S-3p hybridization which appeared clearly in density of states (DOS) results. This indicates that p–d orbital interactions are critical in the control of the valence electronic structure and semiconducting property of CuS. The calculated optical properties also supported a dielectric zero signal at approximately 4.8 eV and low static reflectivity as well as dispersion of the refractive index associated with inter-band transitions and a clear peak in the energy-loss function (approx. 20.9 eV), demonstrating a bulk plasmon response at high energies and without metallic conductivity. Overall, the strong consistency between experimental observations and GGA+U predictions establishes a reliable experimental–theoretical description of hexagonal CuS nanoparticles and highlights their suitability for NIR-driven photothermal conversion, optoelectronic devices, and related energy applications.

Acknowledgment

The authors would like to acknowledge the support of University Littoral Côte d'Opale (ULCO) the, University of Picardie Jules Verne (UPJV) and the College de France through the PAUSE program, which hosted Musleh Hussam and Aldahoudi Naji.

References :

1. Adhikari, S., D. Sarkar, and G. Madras, *Hierarchical Design of CuS Architectures for Visible Light Photocatalysis of 4-Chlorophenol.* ACS Omega, 2017. **2**(7): p. 4009-4021.
2. ul Ain, N., et al., *Copper sulfide nanostructures: synthesis and biological applications.* RSC advances, 2022. **12**(12): p. 7550-7567.
3. Nath, D., F. Singh, and R. Das, *X-ray diffraction analysis by Williamson-Hall, Halder-Wagner and size-strain plot methods of CdSe nanoparticles-a comparative study.* Materials Chemistry and Physics, 2020. **239**: p. 122021.
4. Pathak, S.S. and L.S. Panchakarla, *A large area flexible p-type transparent conducting CuS ultrathin films generated at liquid-liquid interface.* Applied Materials Today, 2021. **24**: p. 101152.
5. Tailor, J.P., S. Chaki, and M. Deshpande, *Comparative study between pure and manganese doped copper sulphide (CuS) nanoparticles.* Nano Express, 2021. **2**(1): p. 010011.
6. Shaat, S., et al., *Inexpensive organic dyes-sensitized zinc oxide nanoparticles photoanode for solar cells devices.* Journal of Photonics for Energy, 2017. **7**(2): p. 025504-025504.
7. Mansy, S., et al., *Computational and experimental study of wurtzite phase ZnO nanoparticles.* Materials Today Communications, 2023. **35**: p. 105688.
8. Yang, W.-Z., et al., *Giant five-shell polyoxometalate cages and the single-cluster-based nanowire superstructures.* Journal of the American Chemical Society, 2025. **147**(29): p. 25990-25997.

9. Chen, Q., et al., *CuS nanosheets as additives in the hole transport layers for stable pin perovskite solar cells.* Nano Energy, 2025. **135**: p. 110652.
10. Deng, J. and Z.-Y. Zhao, *Effects of non-stoichiometry on electronic structure of CuxSy compounds studied by first-principle calculations.* Materials Research Express, 2019. **6**(10): p. 105513.
11. Morales-García, A., et al., *First-principles calculations and electron density topological analysis of covellite (CuS).* The Journal of Physical Chemistry A, 2014. **118**(31): p. 5823-5831.
12. Abbas, Z., et al., *A DFT+ U study of the effect of transition metal replacements on optoelectronic and elastic properties of TmCu3S4 (Tm= V, Ta, Nb).* Optik, 2022. **250**: p. 168289.
13. Khan, M.S., et al., *First-principles study of the electronic structure, optical, thermodynamic, and thermoelectric nature in MgACu 3 Se 4 (A= Sc, Y) semiconductors.* Optical & Quantum Electronics, 2024. **56**(4): p. 1.
14. Córdova-Castro, R.M., et al., *Anisotropic plasmonic CuS nanocrystals as a natural electronic material with hyperbolic optical dispersion.* ACS nano, 2019. **13**(6): p. 6550-6560.
15. Milekhin, A.G., et al., *Combination of surface-and interference-enhanced Raman scattering by CuS nanocrystals on nanopatterned Au structures.* Beilstein journal of nanotechnology, 2015. **6**(1): p. 749-754.
16. Liu, N., et al., *Copper sulfide nanoparticles coated with Fe-EGCG networks for targeted MR imaging and chemo/photothermal/chemodynamic synergetic therapy of tumors.* Biomaterials Science, 2026. **14**(9): p. 2384-2402.
17. An, Q., et al., *Tumor microenvironment activated heptamethine cyanine photosensitizer for In situ CuS nanoparticle generation triggering near infrared fluorescence imaging and synergistic photothermal/photodynamic therapy.* Small, 2026: p. e12555.
18. Kalanur, S.S. and H. Seo, *Tuning plasmonic properties of CuS thin films via valence band filling.* RSC Advances, 2017. **7**(18): p. 11118-11122.
19. Riyaz, S., A. Parveen, and A. Azam, *Microstructural and optical properties of CuS nanoparticles prepared by sol–gel route.* Perspectives in Science, 2016. **8**: p. 632-635.
20. Shaat, S., et al., *Inexpensive organic dyes-sensitized zinc oxide nanoparticles photoanode for solar cells devices.* Journal of Photonics for Energy, 2017. **7**(2): p. 025504.
21. Shaat, S., et al., *Structural parameters of hydrothermally synthesized ZnO nanostructure and their based solar cells.* Nano-Structures & Nano-Objects, 2020. **23**: p. 100515.
22. Han, P., et al., *Nonlinear Electrical Conductivity and Thermal Conductivity of g-C3N4/Liquid Silicone Rubber Field Grading Composites.* Materials, 2026. **19**(11): p. 2367.
23. Suhail, A.M., et al., *Synthesies of ZnO Quantum Dot by by Self assemply Method and ZnO Nanorod by Hydrothermal Method.* International Journal of Advanced Technology in Engineering and Science, 2015. **3**(4): p. 10.
24. Shaat, S.K., H.C. Swart, and O.M. Ntwaeaborwa, *Investigation of luminescent properties of Ca0. 3Sr0. 7Al2O4: Tb3+, Eu3+ excited using different excitation sources.* Journal of Electron Spectroscopy and Related Phenomena, 2014. **197**: p. 72-79.
25. Raveendra, R., et al., *Synthesis, structural characterization of nano ZnTiO3 ceramic: An effective azo dye adsorbent and antibacterial agent.* Journal of Asian Ceramic Societies, 2014. **2**(4): p. 357-365.
26. Shaat, S., et al., *Solution combustion-derived ZnO nanoparticles for photoanode of solar cells.* journal of Materials Science Engineering: B, 2019. **241**: p. 75-81.
27. Hurma, T. and S. Kose, *XRD Raman analysis and optical properties of CuS nanostructured film.* Optik, 2016. **127**(15): p. 6000-6006.
28. Chaki, S.H., J. Tailor, and M. Deshpande, *Covellite CuS–Single crystal growth by chemical vapour transport (CVT) technique and characterization.* Materials science in semiconductor processing, 2014. **27**: p. 577-585.

29. Kushwah, R., et al., *Facile and controlled synthesis of copper sulfide nanostructures of varying morphology.* Journal of Materials Science: Materials in Electronics, 2017. **28**: p. 5597-5602.
30. Ravele, M.P., O.A. Oyewo, and D.C. Onwudiwe, *Controlled synthesis of CuS and Cu9S5 and their application in the photocatalytic mineralization of tetracycline.* Catalysts, 2021. **11**(8): p. 899.
31. Jaggi, N., *Effect of Reaction Temperature on Structural and Optical Properties of CuS Nanoparticles: HYDROMAGNETIC BOUNDARY LAYER FLOW WITH FORCED CONVECTIVE HEAT TRANSFER.* Indian Journal of Engineering and Materials Sciences (IJEMS), 2023. **30**(3): p. 447-451.
32. Selvi, S.S.T., J.M. Linet, and S. Sagadevan, *Influence of CTAB surfactant on structural and optical properties of CuS and CdS nanoparticles by hydrothermal route.* Journal of Experimental Nanoscience, 2018. **13**(1): p. 130-143.
33. Khan, M.S., et al., *The optoelectronic, mechanical, and thermoelectric properties of novel wide band gap double perovskites: a first-principles study.* Scientific Reports, 2025. **15**(1): p. 39816.
34. Conejeros, S., et al., *Nature of holes, oxidation states, and hypervalency in covellite (CuS).* Inorganic Chemistry, 2014. **53**(23): p. 12402-12406.
35. Paliwal, S., V. Maurya, and K. Joshi, *First-principles study of electronic structure and fermiology of covellite mineral and its B1, B3 phases.* Journal of Physics: Condensed Matter, 2020. **32**(29): p. 295501.
36. Oppong-Antwi, L., B. Huang, and J.N. Hart, *Electronic properties of transition and alkaline earth metal doped CuS: A DFT Study.* ChemPhysChem, 2023. **24**(23): p. e202300417.
37. Zhu, J., et al., *Thermal equations of state and phase relation of PbTiO3: A high P-T synchrotron x-ray diffraction study.* Journal of Applied Physics, 2011. **110**(8).
38. Iqbal, M.A., et al., *Unveiling concentration effects on the structural and optoelectronic characteristics of Zn1Àx Cdx S (x ¼ 0, 0.25, 0.50, 0.75, 1) cubic semiconductors: a theoretical study.* 2022.
39. Zharov, A.A., I.V. Shadrivov, and Y.S. Kivshar, *Nonlinear properties of left-handed metamaterials.* Physical Review Letters, 2003. **91**(3): p. 037401.
40. Gautam, L., et al., *Impact of Cu 2 S activity on dielectric properties of oil-paper insulation under different ambient conditions.* IEEE Transactions on Dielectrics and Electrical Insulation, 2025.
41. Ouerghui, W., M.S. Alkhalifah, and H.B. Abdallah, *DFT calculations on ZnO1−x compounds for optoelectronic applications.* Journal of Computational Electronics, 2021. **20**(1): p. 467-479.
42. Islam, M.R., et al., *Hybrid Modeling and Optimization of Cs2SiBr6 Perovskite Solar Cells Using DFT, Machine Learning, and SCAPS-1D Simulation.* Advanced Theory and Simulations, 2026. **9**(3): p. e01685.
43. Xiao, L., et al., *Near-infrared radiation absorption properties of covellite (CuS) using first-principles calculations.* AIP Advances, 2016. **6**(8).
44. Dorothy, A.A. and P. Panigrahi, *First principles study of optical properties of Ni-and Pd-doped TiO2 as visible light catalyst.* Materials for Renewable and Sustainable Energy, 2023. **12**(1): p. 47-52.